Data-Driven Control for Interlinked AC/DC Microgrids via Model-Free Adaptive Control and Dual-Droop Control

Zhang, Huaguang; Zhou, Jianguo; Sun, Qiuye; Guerrero, Josep M.; Ma, Dazhong

Published in:
I E E E Transactions on Smart Grid

DOI (link to publication from Publisher):
10.1109/TSG.2015.2500269

Publication date:
2017

Document Version
Accepted author manuscript, peer reviewed version

Data-Driven Control for Interlinked AC/DC Microgrids via Model-Free Adaptive Control and Dual-Droop Control

Huaguang Zhang, *Fellow, IEEE,* Jianguo Zhou, Qiuye Sun, *Member, IEEE,* Josep M. Guerrero, *Fellow, IEEE,* and Dazhong Ma

***Abstract*—This paper investigates the coordinated power sharing issues of interlinked ac/dc microgrids. An appropriate control strategy is developed to control the interlinking converter (IC) to realize proportional power sharing between ac and dc microgrids. The proposed strategy mainly includes two parts: the primary outer-loop dual-droop control method along with secondary control; the inner-loop data-driven model-free adaptive voltage control. Using the proposed scheme, the interlinking converter, just like the hierarchical controlled DG units, will have the ability to regulate and restore the dc terminal voltage and ac frequency. Moreover, the design of the controller is only based on input/output (I/O) measurement data but not the model any more, and the system stability can be guaranteed by the Lyapunov method. The detailed system architecture and proposed control strategies are presented in this paper. Simulation and experimental results are given to verify the proposed power sharing strategy.**

***Index Terms*—Interlinked microgrids, interlinking converter, power sharing, dual-droop control, data-driven model-free adaptive control.**

NOMENCLATURE

$\Delta\omega_{IC,pu}$	Secondary control frequency signal sent to the primary control level
ΔP_{Lac}	Increased active powers of the ac microgrids at the time of t_k
ΔP_{Ldc}	Increased active powers of the dc microgrids at the time of t_k
$\Delta v_{IC,dc,pu}$	Secondary control voltage signal sent to the primary control level
η	Threshold of the deviation
$\omega^*_{ac,pu}$	Nominal frequency of the ac microgrid
$\omega^*_{IC,pu,t_{k+1}}$	Reference frequency of the IC
$u(\cdot)$	Unit step function
$V^*_{dc,pu}$	Nominal voltage of the dc microgrid
$V^*_{IC,dc,pu,t_{k+1}}$	Reference dc voltage of the IC
$\bar{\omega}_{ac,pu}$	The average frequency of the ac microgrid
$\bar{V}_{dc,pu}$	The average voltage of the dc microgrid
Λ_σ	Update factor of the droop coefficient when the power transferred to the ac microgrid
Λ_k	Update factor of the droop coefficient when the power transferred to the dc microgrid
$\omega_{ac,pu,t_{k+1}}$	Measured terminal ac frequency at the time of t_{k+1}
$\tilde{\sigma}_{IC,t_k}$	Droop coefficient of the IC when the power transferred to the ac microgrid
$\tilde{k}_{IC,t_k}$	Droop coefficients of the IC when the power transferred to the dc microgrid
φ_{ac}	Active power that should be shared by the ac microgrids
φ_{dc}	Active power that should be shared by the dc microgrids
C_{dc}	Dc-link capacitance of the IC
C_{IC_f}	Filter capacitance of the IC
d_u	Unknown input order of the IC system
d_y	Unknown output order of the IC system
$f_i(\cdot)$	Unknown nonlinear function vectors of the IC system
i_{IC_abc}	Ac currents of filter inductance of the IC
i_{IC_dc}	Dc-link input current of the IC
k_{ac}	Combined droop coefficient of the ac microgrid
k_{dc}	Combined droop coefficient of the dc microgrid
$k_{i\omega}$	The integral gain of the secondary frequency controller
k_{iV}	The integral gain of the secondary dc voltage controller
$k_{p\omega}$	The proportional gain of the secondary frequency controller
k_{pV}	The proportional gain of the secondary dc voltage controller
L_{IC_f}	Filter inductance of the IC
P_{IC,t_K}	Active power transferred by the IC at the time of t_k
R_{IC_f}	Filter resistance of the IC
u_{abc_ave}	Average switching signals of the IC
$V_{dc,pu,t_{k+1}}$	Measured dc microgrid voltage at the the time of t_{k+1}
$V_{IC,dc}$	Dc-link voltage of the IC
$v_{IC\_o\_abc}$	Ac voltages of filter capacitor of the IC

This work was supported in part by the National Natural Science Foundation of China under Grant 61433004, Grant 61573094, in part by the Fundamental Research Funds for the Central Universities under Grant N140402001, in part by IAPI Fundamental Research Funds under Grant 2013ZCX14, and in part by the Development Project of Key Laboratory of Liaoning Province.

H. Zhang is with the School of Information Science and Engineering, Northeastern University, Shenyang 110819, China. He is also with the Key Laboratory of Integrated Automation of Process Industry (Northeastern University) of the National Education Ministry, Shenyang 110819, China (e-mail: hgzhang@ieee.org).

J. Zhou, Q. Sun and D. Ma are with the School of Information Science and Engineering, Northeastern University, Shenyang 110819, China (e-mail: JianguoZhou.NEU@gmail.com; sunqiuye@ise.neu.edu.cn; madazhong@ise.neu.edu.cn).

J. M. Guerrero is with the Department of Energy Technology, Aalborg University, Aalborg 9220, Denmark (e-mail: joz@et.aau.dk).

I. INTRODUCTION

DUE to the fast proliferation of distributed generators (DGs) in power systems, managing the power of different DGs and the grid has become crucial, and microgrid provides a promising solution. Therefore, focus on ac and dc microgrids has grown rapidly with their architectural [1], [2], modeling [3], stability analysis and enhancement [4]-[6], power quality improvement [7]-[9], power sharing control [10]-[13], and other issues. Most developments mentioned above on microgrids are, however, directed at DG control mainly within one microgrid.

Enforcing ac and dc microgrids intertied by an interlinking power converter is a promising topology in future power networks, and has in fact been discussed recently due to some benefits, such as greater security and reliability, and reduced transmission and distribution losses [14]. Autonomous operation and modified droop control schemes of such hybrid microgrids were discussed in [15], [16] and extended in [17], [18] by integrating an energy storage system to the dc microgrid. Another droop control scheme was followed in [19] for bidirectional power flow between the intertied microgrids. In [20], hierarchical control of multiple parallel ac-dc converter interfaces between ac and dc buses was proposed to achieve proportional current sharing.

Despite the progress mentioned above, some drawbacks of the previous methods can also be found. (i) The majority of the existing inner loop control techniques are greatly dependent on mathematical model. These techniques cannot give satisfactory results when suffering poor model. Uncertainty dynamics and disturbances [21], [22] widely exist in inverter-based microgrids, and it is difficult to obtain the accurate model. Although robust control [23], predictive control [24], variable-structure control [25], and neural network [26] -based control have been proposed for power converters, some challenges still exist. Partial mathematical model and uncertainty dynamics should be known for design of robust controller and variable-structure controller. While predictive control has good performance and strong robustness, the model or structure of the plant also should be known. (ii) Proportional power sharing and voltage (frequency) regulation cannot be achieved at the same time. Interlinking converters in [14] and [18] can be viewed as voltage sources, but proportional power sharing between two microgrids cannot be achieved accurately. On the other hand, in [16], [17] and [19], interlinking converters can be viewed as current sources since they are current controlled converters, which implies these interlinking converters cannot participate in voltage and frequency regulation. (iii) Although various secondary control schemes have been developed to restore the frequency and voltage to their nominal values, the restoration of ac frequency and dc voltage has not been considered in the previous literatures for the interlinked ac and dc microgrids, such as [15]-[19]. Therefore, a new appropriate control scheme should be further developed for interlinking converts to address these issues mentioned above.

Obtaining the system model information that is accurate enough is very difficult in such complicated interlinked microgrid systems. It is more important and meaningful to take advantage of the large amount of the process data produced by the system to boost the operating efficiency and cut the costs. Data-driven model-free adaptive control (DDMFAC) does not require any model information of the controlled plant and the required control performance can be achieved by using the input/output (I/O) data. It is of great significance to take advantage of the process data in such complex system particularly for the future smart grid and energy internet.

This paper presents a data-driven control (DDC) structure for interlinking converters in interlinked ac and dc hybrid microgrids. One important reason that we try to use the data-driven MFAC method to design the controller of the IC in the paper is to take the most advantage of the process data, boost the efficiency, and cut the costs on the basis of achieving required control performance. The proposed control scheme employs a data-driven model-free adaptive voltage controller (DDMFAVC) for fast and robust voltage tracking and a dual-droop controller with a secondary controller for proportional coordinated power sharing between ac and dc microgrids and restoration of frequency and dc voltage. Considering the voltage controller, model-free adaptive control (MFAC) perhaps is the best solution. Firstly, MFAC does not require a mathematical model, order, structure information or time delay of the controlled plant but only input/output (I/O) measurement data [27], which implies that a generic controller can be designed and developed independently for interlinking converters in practice. Secondly, the pseudo partial derivative (PPD) behavior of MFAC may not be sensitive to the variations of the parameter, structure, or delay of the controlled system. Therefore, MFAC scheme has strong robustness which is the key requirement of interlinking converters. Finally, DDC (MFAC) has been successfully implemented in some practical fields [28]-[31]. Based on the aforementioned consideration, a newly designed data-driven MFAC scheme is proposed for the interlinking converter.

A dual-droop controller is also proposed in this paper, and the main reasons are kindly summarized as: (i) In the wider scope of power sharing, source capabilities can be shared among different types of microgrids, and individual source variations can be always kept small regardless of where the load transients are triggered. These advantages cannot be realized by just relying on the droop-controlled DGs within each microgrid. It would certainly rely on the coordinated operation of dc sources, ac sources, and interlinking converters. Emphasis should be equally given to the interlinking converter. (ii) More complex supply-demand scenarios should be considered when the interlinked microgrids operate in the islanding mode since the infinite mains is no longer there to cushion any unbalance and load variations. In the islanding mode, sources can no longer produce maximum or optimal powers continuously. They should not only share the load power but also participate in the frequency and voltage regulation which is extremely important for the stable operation of the interlinked microgrids. It is, therefore, necessary and significant to allow the interlinking converter to regulate the frequency and voltage. (iii) Some droop control schemes have been proposed [14]-[19]. However, proportional power sharing, dc voltage and ac frequency regulation cannot be achieved at the same time by using the previous droop methods. Interlinking converters in [14] and [18] can be viewed as

voltage sources, but proportional power sharing between two microgrids cannot be achieved accurately. On the other hand, in [16], [17] and [19], interlinking converters can be viewed as current sources, which implies these interlinking converters cannot participate in voltage and frequency regulation. The proposed dual droop control method in our paper can address these problems, allowing the interlinking converter to regulate the ac voltage and frequency and dc voltage while keeping proportional power sharing. The main contribution of this paper can be summarized as follows:

1) A novel data-driven model-free adaptive voltage control (DDMFAVC) scheme is introduced for interlinking converters in interlinked ac and dc hybrid microgrids. The model, structure, uncertainty dynamics, and unmodeled dynamics are not required in this scheme.

2) Dynamic dual-droop control scheme is proposed to achieve proportional power sharing between ac and dc microgrids. This droop scheme, along with the voltage controller, enables proportional power sharing and voltage/frequency regulation realized simultaneously like DGs in microgrids.

3) A novel secondary control strategy is proposed for the interlinked ac and dc microgrids, which is different from that of DGs in microgrids.

The remainder of this paper is structured as follows. The interlinked ac and dc hybrid microgrids are presented in Section II. The proposed control scheme is presented in Section III. Simulation and experimental results are presented in Section IV and Section V, respectively. Conclusions are finally drawn in Section VI.

II. System Structure and Modeling of Interlinking Converter

A. System Structure and Operation Modes

The considered interlinked ac and dc microgrids are shown in Fig. 1, in which an interlinking converter (IC) is utilized to link the ac and dc microgrids together. Each microgrid has its own sources, storages and loads. The interlinking converter, between the two microgrids, is to provide bidirectional power transfer depending on present generating and loading conditions of each microgrid. The formed interlinked microgrids can be tied to the utility grid through a solid state transformer (SST) based energy router [32]. In the grid-connected mode, the energy router can operate as a constant power source [18] seen from the main utility grid side, injecting (or absorbing) constant active power to (or from) the utility grid so as to not to disturb the main utility grid unnecessarily. It means that for the main utility grid, the distributed energy sources will become "controllable", which is great beneficial to the stability of the main utility grid. The interlinking converter, in both grid-connected and islanded modes, will provide bidirectional power transfer to participate in proportional power sharing between the two microgrids by using the proposed dual-droop control. Sources should decide on the right amount of energy to produce to meet the load demand rather than produce maximum or optimal powers continuously in both grid-connected and islanded modes. In this paper, three operation modes of the interlinking converter are considered as follows.

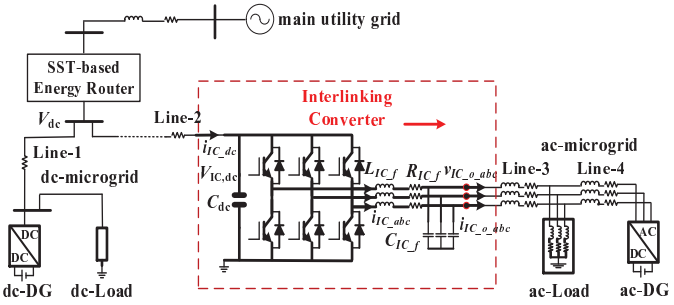

Fig. 1. An example of interlinked ac/dc microgrids.

Mode-1: If the determined active power is negative, it means that the $V_{IC,dc} - P$ droop is selected and that the interlinking converter will absorb the power from the ac microgrid and then inject into the dc microgrid. The interlinking converter, seen from the dc-link side, just acts as a "dc DG" unit in this mode.

Mode-2: If the determined active power is positive, it means that the $\omega_{IC} - P$ droop is selected and that the interlinking converter will inject the power to the corresponding ac microgrid. The interlinking converter takes the same role of an "ac DG" as that in the ac microgrid in this mode.

Mode-3: There will be no power transferred by the interlinking converter when both the ac and dc microgrids are underloaded or over-loaded, or some faults occur, or deviation of the per-unit values of dc voltage and ac frequency is less than threshold.

B. Dynamic Linearization Data Model of IC

Usually, a voltage source inverter (VSI) can be adopted for the interlinking converter. And a sample configuration is shown in Fig. 1. In natural reference frame, considering the dc-link voltage dynamics and ignoring conducting resistances of the switching devices in the IC, the complete average switching dynamics of the interlinking converter can be given by

$$\begin{aligned} \dot{V}_{IC,dc} &= (1/C_{dc})\, i_{IC\_dc} - (1/C_{dc}V_{IC,dc})\, \mathbf{u}_{abc\_ave}^{T} \mathbf{i}_{IC\_abc} \\ \dot{\mathbf{i}}_{IC\_abc} &= (-R_{IC\_f}/L_{IC\_f})\, \mathbf{i}_{IC\_abc} \\ &\quad + (1/L_{IC\_f})\, (V_{IC,dc}\mathbf{u}_{abc\_ave} - \mathbf{v}_{IC\_o\_abc}) \\ \dot{\mathbf{v}}_{IC\_o\_abc} &= (1/C_{IC\_f})\, (\mathbf{i}_{IC\_abc} - \mathbf{i}_{IC\_o\_abc}) \end{aligned} \tag{1}$$

where $\mathbf{i}_{IC\_abc}$, $\mathbf{v}_{IC\_o\_abc}$, $\mathbf{u}_{abc\_ave}$, and $\mathbf{i}_{IC\_o\_abc}$ are ac currents of filter inductance, ac voltages of filter capacitor, average switching signals and ac output currents of the interlinking converter, respectively. $V_{IC,dc}$ and i_{IC_dc} are dc-link voltage and input current, respectively. L_{IC_f}, R_{IC_f}, C_{IC_f} and C_{dc} are the filter inductance, filter resistance, filter capacitance, and dc-link capacitance, respectively. We choose $V_{IC,dc}$ and $\mathbf{v}_{IC\_o\_abc}$ as the system outputs when the interlinking converter operates in mode-1 and mode-2, respectively, and $\mathbf{u}_{abc\_ave}$ as the system control inputs. Then the dynamics, for digital implementation, can be expressed in a discrete-time

domain with the conversion $H(s)=\left(1-e^{-sT}\right)/s$ as

$$\begin{aligned}\mathbf{v}_{IC\_o\_abc}(k+1)=&\mathbf{f}_1\left(\mathbf{v}_{IC\_o\_abc}(k),\cdots,\mathbf{v}_{IC\_o\_abc}(k-d_{y1})\right.\\&\left.,\mathbf{u}_{abc\_ave}(k),),\cdots,\mathbf{u}_{abc\_ave}(k-d_u)\right)\\V_{IC,dc}(k+1)=&f_2\left(V_{IC,dc}(k)\cdots,V_{IC,dc}(k-d_{y2}),\right.\\&\left.\mathbf{u}_{abc\_ave}(k),\cdots,\mathbf{u}_{abc\_ave}(k-d_u)\right)\end{aligned}\tag{2}$$

where $\mathbf{v}_{IC\_o\_abc}=\left[v_{IC\_o\_a},v_{IC\_o\_b},v_{IC\_o\_c}\right]^T$, $\mathbf{u}_{abc\_ave}=\left[u_{a\_ave},u_{b\_ave},u_{c\_ave}\right]^T$. Let $\mathbf{V}_1=\mathbf{v}_{IC\_o\_abc}$, $\mathbf{V}_2=V_{IC,dc}$, $\mathbf{u}=\mathbf{u}_{abc\_ave}$, and $\mathbf{f}_2=f_2$, then the dynamics in (2) can be expressed as

$$\begin{aligned}\mathbf{V}_i(k+1)=&\mathbf{f}_i\left(\mathbf{V}_i(k),\cdots,\mathbf{V}_i(k-d_y),\mathbf{u}(k),\right.\\&\left.\cdots,\mathbf{u}(k-d_u)\right),i=1,2\end{aligned}\tag{3}$$

where d_y and d_u are the unknown orders, and $\mathbf{f}_i(\cdot)$ are unknown nonlinear function vectors.

As mentioned in the previous section, uncertainty dynamics, unmodeled dynamics, and disturbances widely exist in the interlinked microgrids, and it is difficult to obtain the unknown nonlinear function vector $\mathbf{f}_i(\cdot)$. Therefore, data-driven-based partial form dynamic linearization (PFDL) can be the best to be adopted in this paper to obtain the equivalent dynamic linearization data model of system (3).

The implementation of the data-driven MFAC method is usually based on two assumptions: 1) The partial derivatives of with respect to control inputs are continuous; 2) System (2) is generalized Lipschitz. These assumptions imposed on the controlled system are reasonable and acceptable from a practical viewpoint. Assumption 1 is a typical condition of control system design for general nonlinear systems. Assumption 2 limits the rates of changes of the system outputs driven by the changes of the control inputs. From the 'energy' point of view, the output energy change rates inside a system cannot go to infinity if the changes of the control input energy are in a finite altitude. According to these assumptions and Theorem 1 in [27], for the nonlinear system (3), there must be parameters $\mathbf{\Phi}_i(k),\forall i=1,2$ called (pseudo partitioned Jacobian matrix, PPJM), and system (3) can be transformed into the following PFDL description when $\|\Delta\mathbf{U}(k)\|\neq 0$:

$$\Delta\mathbf{V}_i(k+1)=\mathbf{\Phi}_i(k)\Delta\mathbf{U}(k),\forall i=1,2\tag{4}$$

where each variable is given in Appendix A.

III. Proposed Control Scheme

A. Data-Driven Model-Free Adaptive Voltage Controller

Based on the PFDL system (4), the DDMFAVC controller for the interlinking converter can be designed in the following. Before giving out the controller, an observer is proposed to estimate the parameters $\mathbf{\Phi}_i(k)$ (PPJM), and the observer and the adaptive update law for $\mathbf{\Phi}_i(k)$ are given by

$$\begin{aligned}\hat{\mathbf{V}}_i(k+1)&=\hat{\mathbf{V}}_i(k)+\hat{\mathbf{\Phi}}_i(k)\Delta\mathbf{U}(k)+\mathbf{K}_i\tilde{\mathbf{V}}_i(k)\\\hat{\mathbf{\Phi}}_i^T(k+1)&=\hat{\mathbf{\Phi}}_i^T(k)+\mathbf{\Gamma}_i(k)\\&\quad\left(\tilde{\mathbf{V}}_i(k+1)-\mathbf{F}_i\tilde{\mathbf{V}}_i(k)\right)\Delta\mathbf{U}(k)\mathbf{I}_{1\times 3L}\end{aligned}\tag{5}$$

where all the variables are given in Appendix A.

Upon the parameters $\mathbf{\Phi}_i(k)$ estimated, the DDMFAVC controller can be designed as

$$\begin{aligned}&\mathbf{u}(k)=\mathbf{u}(k-1)+\hat{\mathbf{\Phi}}_i^T(k)\left[\alpha_i+\hat{\mathbf{\Phi}}_i(k)\hat{\mathbf{\Phi}}_i^T(k)\right]^{-1}\\&\times\left[\mathbf{V}_i^*(k+1)-\hat{\mathbf{V}}_i(k)-\mathbf{K}_i\tilde{\mathbf{V}}_i(k)\right],for\,\|\Delta\mathbf{U}(k)\|\leq\delta\\&\mathbf{u}(k)=\mathbf{u}(k-1)+\delta\cdot sign\left(\Delta\mathbf{u}(k)\right),\text{for}\,\|\Delta\mathbf{U}(k)\|>\delta\end{aligned}\tag{6}$$

where $\alpha_i=diag(\alpha_1,\alpha_2,\alpha_3)$, $\alpha_2=\alpha_4$, and $\mathbf{V}_i^*(k)$ are the reference trajectories.

The stability of the proposed DDMFAVC closed-loop control system (6) can be guaranteed by using the Lyapunov-based stability theory. Detailed proof can be found in [31].

It is worthwhile to remark here that the designed voltage controller (5) and (6), unlike the robust controller [23], predictive controller [24], et al., can be obtained and implemented easily only by using input-output data through the data-driven control theory. Mathematical models are not required in the design of the proposed controller. The controller is a lower cost controller since it does not require any external testing signals and any training process. It is simple and implemented easily and flexibly with small computational burden. It is also suitable to complex and large-scale practical systems particularly for the interlinked microgrids since the structure of the plant is often difficult to determine and the parameters are hard to identify and necessary process information that the data-driven MFAC needs can be directly extracted from huge amounts of process data. On the other hand, the voltage controller can be implemented flexibly under different operation modes that are determined by the dual-droop controller discussed in detail in the following subsection. Additionally, with respect to the voltage controller design, complex coordinate transformation can be avoided.

B. Dual-Droop Controller

Proportional power sharing is necessary. In this paper, all the DGs in each microgrid are seen as a larger equivalent controllable distributed generator by summing all their respective source characteristics. The power ratings and loads of microgrids are usually different in practice. Consequently, this allows back-up reserve with each microgrid to be reduced considerably and overstress of each microgrid to be avoided as well, resulting in greater reliability.

Despite the well-recognized droop control strategies in standalone ac or dc microgrids, proper power sharing among multiple microgrids tied together through the interlinking converter cannot be achieved by the conventional droop methods. Considering the statements in Section I, to achieve proportional power sharing between the interlinked microgrids and participate in voltage and/or frequency regulation simultaneously just like DGs in microgrids, a dynamical dual-droop control scheme with power management and distribution is proposed in this paper. The proposed dual-droop control characteristics of the interlinking converter for active power sharing are drawn in Fig. 2. Their mathematical representations are given as

$$P_{IC,t_k}=\begin{cases}\left(\omega_{IC,pu,t_k}^*-\omega_{IC,pu,\max}\right)/\tilde{\sigma}_{IC,t_k}\\\left(V_{IC,dc,pu,t_k}^*-V_{IC,dc,pu\max}\right)\Big/\tilde{k}_{IC,t_k}\end{cases}\tag{7}$$

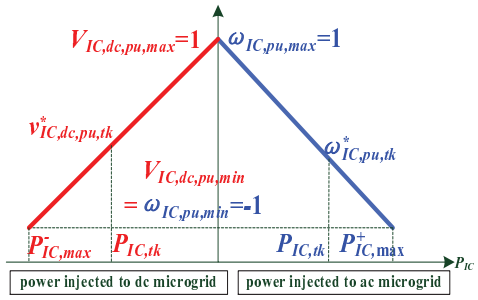

Fig. 2. The proposed dual-droop control characteristics of the interlinking converter.

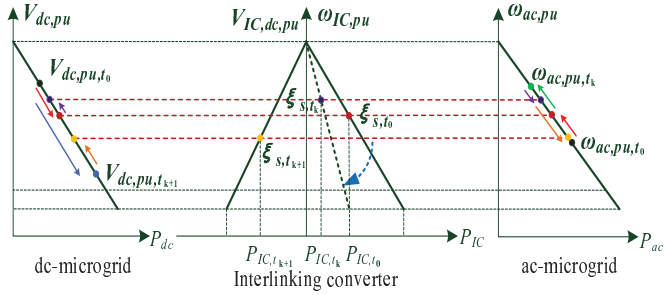

Fig. 3. Illustration of proportional power sharing process realized within the intertied ac and dc microgrids.

where $\tilde{\sigma}_{IC,t_k}$ and $\tilde{k}_{IC,t_k}$ are the active droop coefficients, and "pu" represents the per-unit values that are defined by applying the expressions in [17].

For the appropriate power flow decisions using only variables measured locally, different thresholds can then be set for the frequencies and voltages to distinguish when the microgrids are under-loaded (UL), normal-loaded (NL), or overloaded (OL) in terms of active powers. Using the proposed dual-droop control, the interlinking converter will have three operation modes defined in Section II, and at any instant it just operates at one mode.

Conventionally, within the ac microgrid for example, active and reactive powers at the source terminals are measured for determining reference values for its frequency and voltage magnitude. However, the active power command of the interlinking converter in this paper is determined by the proposed power management and distribution module. Underlying principles of this new droop control scheme can better be understood by referring to the example drawn in Fig. 3. In that figure, the droop lines drawn in the left and right sides are for representing the normalized consolidated droop responses of the ac and dc microgrids given as

$$\begin{aligned} \omega_{ac,pu} &= \omega_{o,pu} - k_{ac}P_{ac} \\ V_{dc,pu} &= V_{o,pu} - k_{dc}P_{dc} \end{aligned} \tag{8}$$

where k_{ac} and k_{dc} are droop coefficients.

When the interlinking converter starts to operate at first time, the interlinking converter will "know" the operating conditions of the two microgrids by measuring the local terminal ac frequencies and dc voltages. For instance, they initially operate at ω_{ac,pu,t_0} and V_{dc,pu,t_0}, respectively, corresponding to the black dots shown in Fig. 3. According to droop control principle, achieving proportional power sharing between the ac and dc microgrids means maintaining $\omega_{ac,pu} = V_{dc,pu} = \xi_s$, corresponding to the red dashed horizontal line drawn in Fig. 3. Therefore, equation (9) can be obtained.

$$\omega_{ac,pu,t_0} + k_{ac}P_{IC,t_0} = V_{dc,pu,t_0} - k_{dc}P_{IC,t_0} \tag{9}$$

where P_{IC,t_0} is the determined active power to be transferred through the interlinking converter for proportional power sharing at $t = t_0$. P_{IC,t_0} can be rewritten as

$$P_{IC,t_0} = \frac{V_{dc,pu,t_0} - \omega_{ac,pu,t_0}}{k_{ac} + k_{dc}} \tag{10}$$

Upon reaching the steady state, proportional active power sharing between different types of microgrids in the interlinking converter enabled system can be realized due to the same vertical axis values ($\omega_{ac,pu} = V_{dc,pu} = \xi_s$) of the consolidated droop lines.

After that, when the loads in the ac and dc microgrids changes, the active power command will be updated using the following equation

$$\begin{aligned} P_{IC,t_{k+1}} &= P_{IC,t_k} - \underbrace{\frac{k_{ac}}{k_{ac}+k_{dc}}\Delta P_{Lac}}_{\varphi_{dc}} + \underbrace{\frac{k_{dc}}{k_{ac}+k_{dc}}\Delta P_{Ldc}}_{\varphi_{ac}} \\ &= \tfrac{1}{k_{ac}+k_{dc}}\left(V_{dc,pu,t_{k+1}} - \omega_{ac,pu,t_{k+1}}\right), k \geq 0 \end{aligned} \tag{11}$$

where P_{IC,t_k} represents the active power to be transferred by the interlinking converter when loads changed at the time $t = t_k$, ΔP_{Lac} and ΔP_{Ldc} represent the increased active powers of the ac and dc microgrids at the time $t = t_{k+1}$, respectively, φ_{ac} and φ_{dc} represent the active power that should be shared by the ac and dc microgrids, respectively, and $\omega_{ac,pu,t_{k+1}}$, $V_{dc,pu,t_{k+1}}$ are the measured terminal ac frequency and dc voltage at the present time $t = t_{k+1}$.

Considering the defined operation modes and thresholds, a more general expression of (11) can be given as

$$P_{IC,t_k} = \begin{cases} 0, & when\ V_{dc,pu,t_k}, \omega_{ac,pu,t_k} \\ & \in (\xi_{UL}, \xi_{\max}] \cup [\xi_{\min}, \xi_{OL}] \\ \frac{1}{k_{dc}+k_{ac}}\left(V_{dc,pu,t_k} - \omega_{ac,pu,t_k}\right), & others \end{cases}. \tag{12}$$

Seen from equation (7) and (12), the interlinking converter monitors the operating of the ac and dc microgrids, and updates the active power command in real time only using the measured ac frequency and dc microgrid voltage. Upon the determined active power $P_{IC,t_{k+1}}$ transferred by the interlinking converter, proportional active power sharing between the ac and dc microgrids can be realized. However, it should be noted that using Eq. (12) will cause almost continuous operation of the interlinking converter for any load variations that will result in more power loss in the converter. Moreover, when the deviation is small enough, it is not necessary for the interlinking converter to transfer the active power. The main reason can be summarized as: 1) the determined active power is too small and much of that will be loosed in the converter under this condition; 2) reliable operation of the system cannot be affected even if the determined active power is not transferred by the interlinking converter. Therefore, to

avoid this, threshold of the deviation is introduced into Eq. (12), and then Eq. (12) can be rewritten as follows:

$$P_{IC,t_k} = \frac{1}{k_{ac}+k_{dc}} \left(V_{dc,pu,t_k} - \omega_{ac,pu,t_k}\right) u\left(\left|V_{dc,pu,t_k} - \omega_{ac,pu,t_k}\right| - \eta\right) \quad (13)$$

where $u(\cdot)$, is the unit step function, η is the threshold of the deviation and it can be expressed as $\eta = f\left(V_{dc,pu,t_k}, \omega_{ac,pu,t_k}\right)$. Eq. (13) can be better and more easily illustrated by using Fig. 8 which is a three-dimensional space Cartesian coordinate reference frame constructed by $V_{dc,pu}$, $\omega_{ac,pu}$ and η. As shown in Fig. 8, the surface S_{ABCD} represents the absolute value of the deviation $\eta_e = |V_{dc,pu,t_k} - \omega_{ac,pu,t_k}|$, and S_{BEJI} and S_{FCHG} represent the over-load and light-load conditions of both the ac and dc microgrids, respectively. S_{EFGHIJ} can be the considered area in some other operation conditions, where active power could not be transferred due to the small deviation. Taking the above into consideration, the surface $S_{B_1E_1F_1C_1H_1I_1}$ is designed to be the threshold $\eta = f\left(V_{dc,pu,t_k}, \omega_{ac,pu,t_k}\right)$ of the deviation in this paper. Thus, when both the ac and dc microgrids are operating in light-load (S_{FCHG}) or over-load (S_{BEJI}) condition, none active power would be transferred from one microgrid to the other due to $\eta_e < \eta$. On the other hand, when the microgrids are operating in the area of S_{EFGHIJ}, the interlinking converter would not transfer any active power due to the small deviation and $\eta_e < \eta$. Therefore, continuous operation of the interlinking converter can be avoided. It is worthy to remark here that the threshold η ($S_{B_1E_1F_1C_1H_1I_1}$) can be flexibly designed according to the requirements of practical applications by using Fig. 7.

As discussed in the literature [16], [17], [19], current-source, rather than voltage-source, characteristics are exhibited by the interlinking converter. In order to participate in voltage and frequency regulation, data-driven model-free adaptive voltage controller is proposed in this paper for the interlinking converter. Therefore, dynamical tuning of the proposed dual-droop lines is indispensable, making the determined reference value $\omega^*_{IC,pu,t_{k+1}}$ or $V^*_{IC,dc,pu,t_{k+1}}$ equal to $\xi_{s,t_{k+1}}$. This can be realized by updating the coefficients of the dual-droop lines using the following equation

$$\begin{aligned} \tilde{\sigma}_{IC,t_{k+1}} &= \Lambda_\sigma \tilde{\sigma}_{IC,t_k}, P_{IC,t_{k+1}} > 0 \\ \tilde{k}_{IC,t_{k+1}} &= \Lambda_k \tilde{k}_{IC,t_k}, P_{IC,t_{k+1}} < 0 \end{aligned} \quad (14)$$

where Λ_σ and Λ_k are given in Appendix B.

The updating process of the active power command and coefficients is also illustrated in Fig. 3.

It can be seen that using the proposed dynamical dual-droop control strategy (7), along with the active power command management and distribution method (13) and the coefficients updating scheme (14), proportional power sharing between the ac and dc microgrids can be realized by the interlinking converter as well as participating in voltage and frequency regulation. The interlinking converter will update the active power command $P_{IC,t_{k+1}}$ and coefficients $\tilde{\sigma}_{IC,t_{k+1}}$ and $\tilde{k}_{IC,t_{k+1}}$ if it "finds" the frequency $\omega_{ac,pu,t_{k+1}}$ of the ac microgrid and/or dc voltage $V_{dc,pu,t_{k+1}}$ of the dc microgrid deviate from the present consensus value ξ_{s,t_k} mainly due to load changing and source changing, reaching at a new consensus state $\xi_{s,t_{k+1}}$.

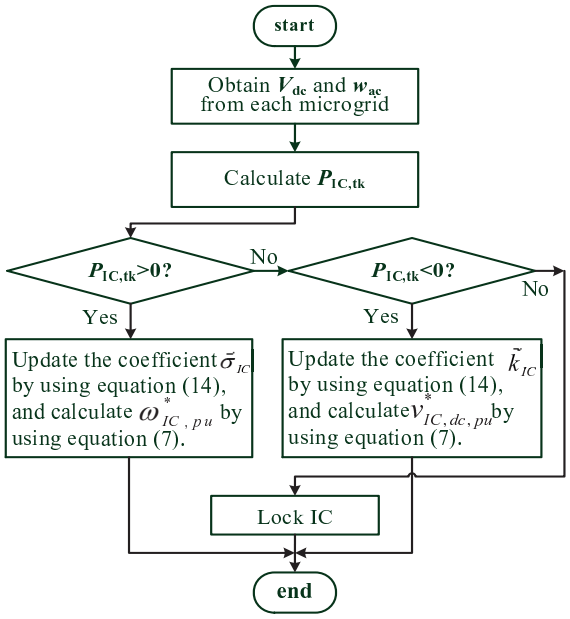

Fig. 4. Illustration of the flow chart of the dual-droop control.

And if the frequency $\omega_{ac,pu,t_{k+1}}$ and dc voltage $V_{dc,pu,t_{k+1}}$ don't change, the active power command $P_{IC,t_{k+1}}$ and coefficients $\tilde{\sigma}_{IC,t_{k+1}}$, $\tilde{k}_{IC,t_{k+1}}$ will be maintained at P_{IC,t_k}, $\tilde{\sigma}_{IC,t_k}$ and $\tilde{k}_{IC,t_k}$, respectively.

Therefore, we could find that the dual-droop control proposed in our paper mainly includes two stages. The first stage is to guarantee the proportional power sharing which can be realized by calculating P_{IC} using equation (13) according to the present load condition of each microgrid. And the second stage is to realize accurate dc voltage and ac frequency regulation which can be achieved by using equation (7) and (14). We admit that droop characteristics similar to [19] and [34] may be obtained if we eliminate P_{IC} from the equation, but it really has some differences. These could be the reason that we use the determined active power P_{IC} as a medium to calculate the references $\omega^*_{IC,pu}$ and $V^*_{IC,dc,pu}$ of the IC. This concept is shown in the flow chart depicted in Fig. 4.

C. Secondary Controller Design

Although droop control method has been widely studied and applied in ac and dc microgrids, conventional droop control can cause frequency and voltage deviation, reducing the reliability and the performance of power sharing. Therefore, various secondary control schemes have been developed to restore the frequency and voltage to their nominal values. Although droop control is used as primary control and non-proportional power sharing schemes are discussed in some papers recently, it should be noted that these works concentrate only on DG control within one microgrid. Regarding the interlinked ac and dc microgrids, the secondary and tertiary control and non-proportional power sharing control used for interlinked microgrids have not been previously investigated by other researchers. In this paper, dual-droop control method is also used as primary control and secondary control scheme are proposed and discussed to achieve proportional power

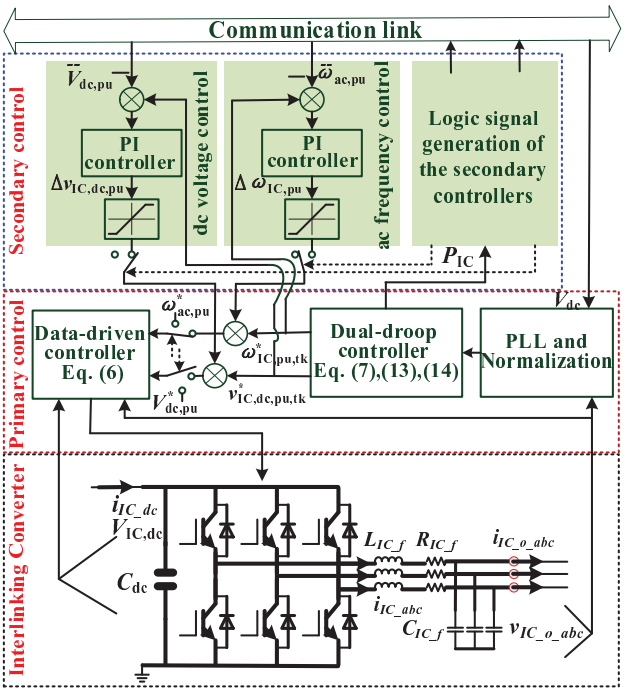

Fig. 5. Details of the secondary controller for the interlinking converter in the hybrid microgrids.

sharing among microgrids, and the distributed secondary control schemes developed in [33] are adopted, which eliminates the design of new secondary controllers for DGs in microgrids. It should be noted that the secondary controller can be avoided in [34] due to its cascaded frequency, angle and virtual torque control topology which makes the VSC emulate the mechanical behavior of a synchronous machine. Thus the VSC can offer synchronization power to eliminate the need for a PLL. Let $\Delta V_{dc,pu} = V^*_{IC,dc,pu} - \bar{V}_{dc,pu}$ and $\Delta\omega_{ac,pu} = \omega^*_{IC,pu} - \bar{\omega}_{ac,pu}$. The distributed secondary controller for the interlinking converter can be expressed as follows:

$$\begin{aligned} \Delta v_{IC,dc,pu} &= k_{pV}\Delta V_{dc,pu} + k_{iV}\int \Delta V_{dc,pu} \\ \Delta\omega_{IC,pu} &= k_{p\omega}\Delta\omega_{ac,pu} + k_{i\omega}\int \Delta\omega_{ac,pu} \end{aligned} \tag{15}$$

where k_{pV}, $k_{p\omega}$, k_{iV} and $k_{i\omega}$ are the PI controller parameters, $\omega^*_{IC,pu}$ and $V^*_{IC,dc,pu}$ are the frequency and voltage of the ac and dc microgrids, respectively, when the synchronization is achieved, $\bar{\omega}_{ac,pu}$ and $\bar{V}_{dc,pu}$ are the average frequency and voltage obtained through the communication network, $\Delta\omega_{IC,pu}$ and $\Delta v_{IC,dc,pu}$ are the secondary control signals sent to the primary control level. A detailed block diagram of the secondary controller of the interlinking converter is shown in Fig. 5.

It is worth noting that the IC can cooperate with the secondary controllers of DGs in each microgrid. It is determined by the logic signals generated by the logic signal generator of the secondary controllers. Details of the flow chart of the logic signal generator is shown in Fig. 6. It is shown that if the dc and ac microgrids are interlinked by the interlinking converter, the secondary controller of DGs in microgrids will be started to restore the dc voltages and ac frequency to their nominal values by cooperating with the IC when some active power is transferred. When each microgrid is operating in islanded mode or no active power is transferred by the interlinking converter, the secondary controllers of DGs will remain working. The deviations of dc voltage and ac frequency will be introduced by droop control when the load changes, resulting in deteriorated power sharing. The power sharing could be improved by restoring the dc voltage and ac frequency through the secondary controller.

The idea of [34] is to develop a cascaded frequency, angle and virtual torque control topology to emulate the mechanical behavior of a synchronous machine which offers synchronization power to eliminate the need for a PLL. Then the VSC dc-link can be viewed as a virtual rotor and some inerter is introduced. Therefore, the VSC has the ability to synchronize with the grid and the frequency can be restored to the preset value under the action of the inerter, which allows the secondary controller to be avoided. The control idea of our paper is based on principle of droop control. The droop controlled DG does not have the inerter existed in the synchronous machine. Therefore, the dc voltage and ac frequency could not be restored to the rated values without the help of the secondary controller. The idea of our paper may be different from that of paper [34].

For the control of dc voltage and omega, due to their dependence [35],the IC can generate the synchronized reference value and send it to the microgrids to be the reference value of the secondary controller. With the help of the secondary controllers of each microgrid, the dc voltage or the ac frequency can be kept stable and almost constant. Thus the dc voltage and omega could be controlled relatively independently to transfer active power. Particularly, the performance will be better if the steady state of the secondary controller can be achieved within fast finite time. Similar method can be found in [36]. When the synchronization between the dc and ac microgrids is achieved, the IC will again generate reference value for the secondary controllers to restore the dc voltages and frequency to their nominal values. In addition, data-driven control method is developed in this paper, which has a good robustness and is not sensitive to the system parameter variation. Therefore, with the help of the secondary controllers, the cooperation between the IC and secondary controllers, and the data-driven method, the dc voltage and omega could be controlled relatively independently. The benefit is that the control could be relatively flexible and that the provision of frequency and dc voltage would be better.

D. Overall Control Diagram

The overall control block diagram showing the realization of the proposed dual-droop control for the interlinking converter can be found in Fig. 7, in which the secondary controller is not included. Firstly, the interlinking converter control is realized by measuring the local ac frequency and dc terminal voltage. These measured variables upon normalized by using the method proposed in [16] are then used to determine the active power command $P_{IC,t_{k+1}}$ (Eq. (13)) for the interlinking converter. According to the determined active power command

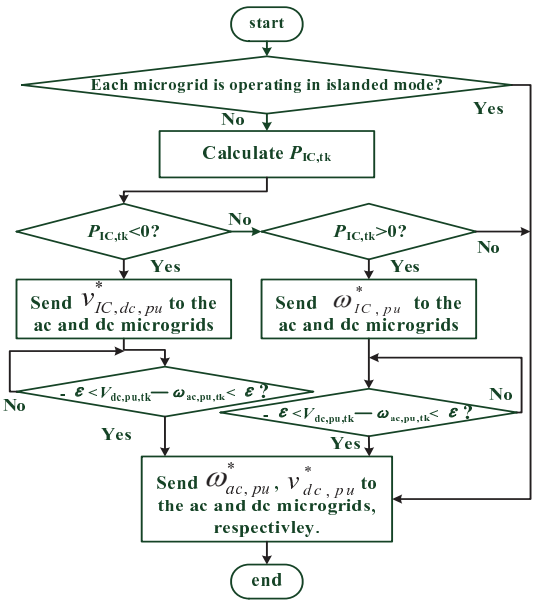

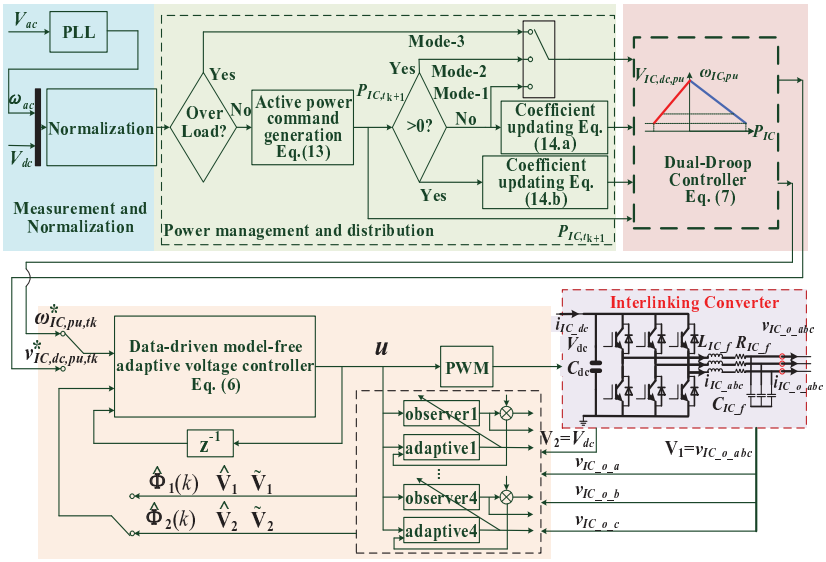

Fig. 6. Flow chart of the logic signal generator of the secondary controllers.

Fig. 7. Overall control diagram for the interlinking converter.

$P_{IC,t_{k+1}}$, the operation mode of the interlinking converter can be selected and then the corresponding coefficient updating signal $\tilde{\sigma}_{IC,t_{k+1}}$ or $\tilde{k}_{IC,t_{k+1}}$ (Eq. (14)) can also be generated. Secondly, using the proposed dual-droop controller (7), along with the active power commands $P_{IC,t_{k+1}}$ and coefficient updating signal $\tilde{\sigma}_{IC,t_{k+1}}$ or $\tilde{k}_{IC,t_{k+1}}$, the references $\omega^*_{IC,pu}$ or $V^*_{IC,dc,pu}$ will be determined. Finally, these references will be given into the inner data-driven model-free adaptive voltage controller.

According to the control diagram, a PLL is used to detect ac frequency for the dual-droop controller. For the inner loop controller, a data driven model-free adaptive controller is designed, which, unlike the conventional PI controller, does not require the ac voltage and current obtained from the coordinate transformation by using the frequency from the PLL. The dynamic I/O data that the DDMFAC requires could be extracted directly from huge amounts of the recorded process data or observer. Maybe, this has nothing to do with PLL directly. The system and controller would not be evidently affected by the PLL that just provides the frequency for the dual-droop controller.

frequency vs. V_{dc} droop in [19] and [34] can be summarized as follows. (i) Compared with [19] where the IC operates in current-controlled mode, the IC with the proposed method in our paper can provide dc voltage and ac frequency support since it is not current-controlled mode. Additionally, communication is adopted in our manuscript to obtain the variables from and send information to the microgrids, respectively. (ii) In [34], the control method was developed from the perspective of SMs, and the dc voltage was controlled by both the frequency and load angle. In our paper, the control method is developed from the perspective of droop control and hierarchical control, and we could control the dc voltage and ac frequency relatively independently with the help of the secondary controllers in each microgrid. (iii) Compared with [19] and [34], accurate active power sharing and synchronization reference signals can be quantitatively guaranteed in theory in this paper. The former is realized by the coefficient $(k_{ac}+k_{dc})^{-1}$ in equation (13) and the latter is realized through equation (7) and (14). (iv) The IC can generate the synchronization reference values to establish the cooperation between the IC and the secondary controllers in each microgrid. Thus both the active power sharing and the restoration of the dc voltage and ac frequency can be realized.

The main advantage of [19] is that it eliminates the need for any communication between microgrids, resulting in relatively fast response, and flexible and convenient design and applications. The advantage of [34] is that the system stability is enhanced due to the introduced virtual inertia and the PLL and secondary controllers are avoided by designing the control topology to emulate the behavior of an SM. However, the advantage of our paper is that the IC can properly provide dc voltage and ac frequency support while keeping accurate proportional active power sharing, which is helpful for the stable operation of the system especially when the system is not connected to the utility grid. The IC can also cooperate with the secondary controllers of DGs in each microgrid by generating synchronization reference values for the secondary controllers thereby helping the microgrid to restore the dc voltages and ac frequency to their nominal values. Another one is that DDC method is adopted in the paper which has a good robustness.

IV. Simulation Results

To validate the performance of the proposed control scheme for the interlinked ac/dc microgrids, the interlinked system, depicted in Fig. 1 has been simulated in MATLAB/Simulink environment. The ac and dc microgrids have its own DGs and loads, and are emulated with a dc-ac inverter and a boost converter, respectively. A six-switch dc-ac converter with

LC filters serving as the interlinking converter is adopted to interface the ac and dc microgrids. Parameters of the system and controllers are presented in Appendix C. To verify the feasibility of the proposed controller, different operating conditions have been considered. From case 1 to case 4, the secondary controllers of the ac and dc microgrids are not considered while this is considered in case 5. Some results are presented and discussed in detail in the following.

A. Case 1

In this case, both the ac and dc microgrids are initially experiencing a load demand of 2 kW each; this means that the two microgrids are initially operating in light load condition. According to the proposed control strategy (13), along with the equal measured per-unit values ($V_{dc,pu} = \omega_{ac,pu} = 0.6$) of the voltage at dc side and the frequency at ac side, no active power (P_{IC,t_k} =0 kW) is transferred by the interlinking converter in this condition. The interlinking converter operates in mode-3. Fig. 9 shows the power responses and the per-unit values of the dc side voltage and the ac side frequency. After t=2 s, loads in the ac and dc microgrids are increased to 5 kW and 7 kW, respectively. In this condition, both the ac and dc microgrids are operating in normal load condition. Thus the per-unit values of the ac side frequency and dc side voltage drop to 0 p.u and -0.4 p.u, respectively. According to (13), $\eta_e > \eta = 0.2$, the active power transferred by the interlinking converter is updated to -1 kW, which means the interlinking converter transfers 1 kW from the ac microgrid to the dc microgrid. The operation mode is changed from mode-3 to mode-1. Upon reaching steady-state, the ac and dc source generations are noted to be the same at about 6 kW each. And the ac and dc microgrids have the same normalized value of -0.2 p.u ($V_{dc,pu} = \omega_{ac,pu} = -0.2$), resulting in proportional power sharing of the total load between the two microgrids.

B. Case 2

Similar to case 1, in this case, the initial load conditions are set to 5 kW for the ac microgrid and 7 kW for the dc microgrid. The interlinking converter transfers 1 kW from the ac microgrid to the dc microgrid in the steady-state described in case 1 to achieve proportional power sharing. At t=3 s, the load demands of the ac and dc microgrids are changed to 8 kW and 6 kW, respectively. Then normalized values of the ac side frequency and dc side voltage are changed to -0.6 p. u and -0.2 p. u, respectively. Upon sensing the mismatch in normalized values, the amount of the active power to be transferred by the interlinking converter is updated to 1 kW according to (13), resulting in the interlinking converter to reverse the power flow with 1 kW shifted from the dc to ac microgrid. Thus the $\omega_{IC,pu} - P$ droop is selected and updated to control the frequency. The operation mode of the interlinking converter is changed from mode-1 to mode-2 now. Fig. 10 shows the power responses and the normalized values of the ac side frequency and the dc side voltage. It can be seen that the total load is proportionally shared between the ac and dc microgrids. In the steady-state, the ac and dc source generations are noted to be the same at about 7 kW each. And the ac and dc microgrids have the same normalized value of -0.4 p. u.

C. Case 3

The over load condition of both the ac and dc microgrids is considered in this case. The initial conditions are set to 8 kW for the ac microgrid and 6 kW for the dc microgrid, respectively. That means the ac microgrid is initially operating in over load condition while the dc microgrid is operating in normal load condition. In the steady state, the interlinking converter transfers 1 kW from the dc microgrid to the ac microgrid, which is discussed in case 2 in detail. At t=3 s, the ac and dc microgrids are changed to 9.5 kW and 9 kW, respectively, which makes both the ac and dc microgrids over loaded. This can also be demonstrated by the measured normalized values (-0.9 p. u and -0.8 p. u). According to (13), the active power to be transferred by the interlinking converter is updated to 0 kW, which means the interlinking converter transfers no power and each microgrid is responsible for the power sharing in this load condition. Fig. 11 shows the power and the normalized values of the ac side frequency and the dc side voltage. It can be seen that the interlinking converter can reasonably manage the power sharing and has a good performance. It is necessary to mention that a loading shedding system may be activated in this condition in practice to guarantee the system stability.

D. Case 4

In this case, the initial conditions are set to 8 kW for the ac microgrid and 6 kW for the dc microgrid, respectively. That means the ac and dc microgrids are initially operating in over load and normal load condition, respectively. In the steady state, the interlinking converter transfers 1 kW from the dc microgrid to the ac microgrid according to Eq. (13). At t=3 s, the ac microgrid is changed to 6.5 kW and the dc microgrid remains 6 kW. Although the ac and dc microgrids are operating at normal load condition, according to (13), the active power to be transferred by the interlinking converter is updated to 0 kW (P_{IC,t_k} =0 kW) since the deviation is less than the threshold ($\eta_e < \eta$), which means the interlinking converter transfers no power and each microgrid is responsible for the power sharing in this load condition. Fig. 12 shows the power and the normalized values of the ac side frequency and the dc side voltage. It can be seen that small deviation of the per-unit values exists between the ac and dc microgrids, and that the interlinking converter can reasonably manage the power sharing and has a good performance.

E. Case 5

Based on case 4, the secondary control scheme is added in this case. The load conditions considered in this simulation is the same as that in case 4. Fig. 13 shows the simulation results, from which it can be seen that the per-unit values of the ac frequency and dc voltage are restored to zero corresponding to their nominal values with help of the secondary controllers. Specifically, at t=2.1 s, synchronization is achieved between the ac and dc microgrids, and the per-unit values of dc voltage and ac frequency meet the condition of $|V_{dc,pu,t_k} - \omega_{ac,pu,t_k}| < \varepsilon = 0.1$. Therefore, the IC sends

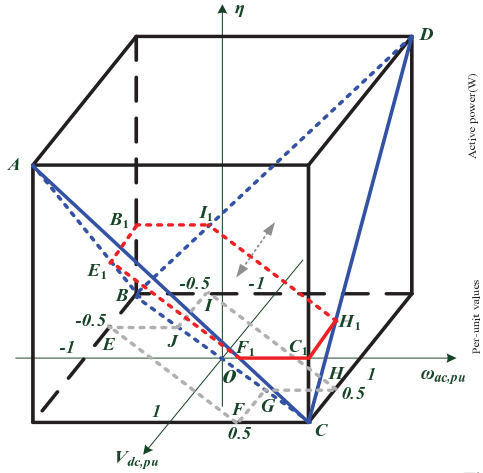

Fig. 8. The schematic diagram of design of the threshold.

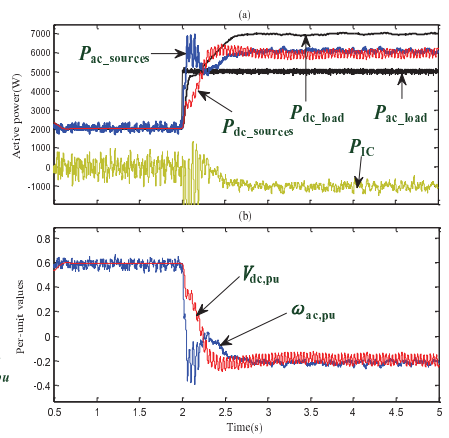

Fig. 9. Power responses and per-unit values. (a) Active power (W). (b) per-unit values of the dc side voltage and ac side frequency.

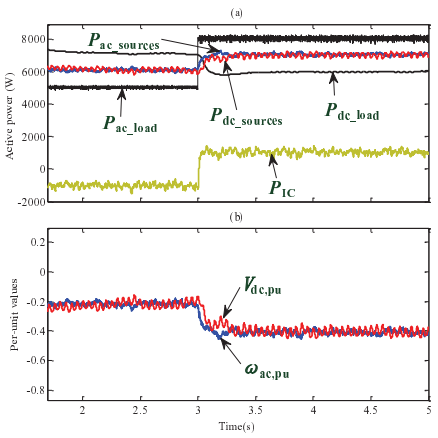

Fig. 10. Power responses and per-unit values. (a) Active power (W). (b) per-unit values of the dc side voltage and ac side frequency.

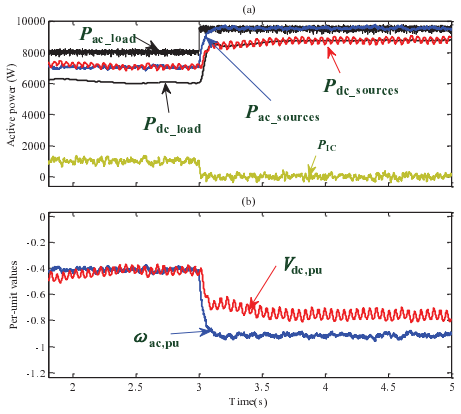

Fig. 11. Power responses and per-unit values. (a) Active power (W). (b) per-unit values of the dc side voltage and ac side frequency.

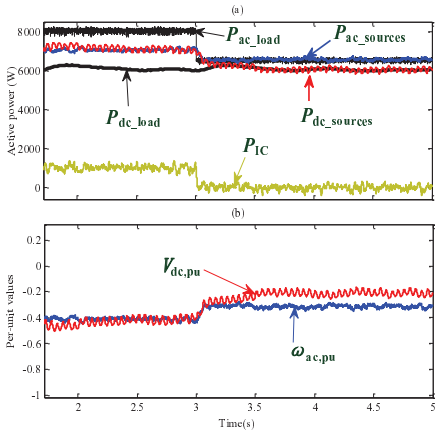

Fig. 12. Power responses and per-unit values. (a) Active power (W). (b) per-unit values of the dc side voltage and ac side frequency.

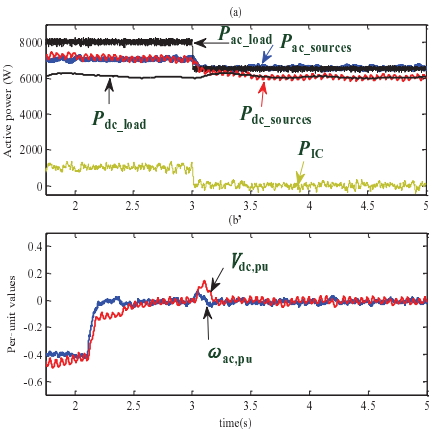

Fig. 13. Power responses and per-unit values. (a) Active power (W). (b) per-unit values of the dc side voltage and ac side frequency.

signals to the ac and dc microgrids to change the reference values of the secondary controllers. Then, the secondary controllers of the DGs in microgrids are started to restore the dc voltage and ac frequency to their nominal values. At t=3 s, the ac microgrid is changed to 6.5 kW and the dc microgrid remains 6 kW. In this load condition, no active power is transferred by the interlinking converter since the deviation is less than the threshold ($\eta_e < \eta$), which means each microgrid is responsible for the power sharing. Therefore, the secondary controller of the interlinking converter is stopped to work and the secondary controllers in each ac and dc microgrid remain working. The dc voltages and the ac frequency in dc and ac microgrids can be kept at their nominal values, respectively.

V. Experimental Results

For verifying the practicality of the proposed scheme, a test interlinked ac and dc microgrid system shown in Fig. 14 was built in the laboratory, comprising an ac microgrid and a dc microgrid. The ac microgrid and the dc microgrid is connected through the interlinking converter. The ac microgrid consists

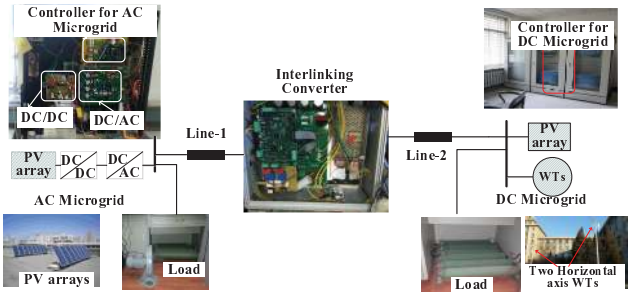

Fig. 14. The tested interlinked ac and dc microgrids.

of 10 kW PV arrays, meanwhile the dc microgrid consists of 5 kW PV arrays and two 5 kW horizontal axis WTs. The light load condition, normal load condition and overload condition are considered for two interlinked microgrids.

Note that ratings of the two microgrids were intentionally set the same with that of the simulation to demonstrate their equally satisfactory responses. Under proportional active power sharing, the p.u. values of the ac frequency and dc

voltage, normalized with respect to their ratings, were always the same in the steady state. The experiment was divided into four stages:

Firstly, the load in the ac microgrid is 5 kW and the load in the dc microgrid is 7 kW which means the two microgrids are operated under normal load condition and the ac microgrid should transfer 1 kW from ac microgrid to dc microgrid through the interlinking conventer; Secondly, the load in ac microgrid is changed to 8 kW and the load in dc microgrid is changed to 6 kW which means the two microgrid are also operated under normal load condition and the dc microgrid should transfer 1 kW to ac microgrid through the interlinking conventer; Thirdly, the load in ac microgrid is changed to 9.5 kW and the load in dc microgrid is changed to 9 kW which means the two microgrid are also operated under overload condition and there is no power through the interlinking conventer; Fourthly, the load in ac microgrid is changed to 6.5 kW and the load in dc microgrid is changed to 6 kW which means the two microgrid are also operated under normal load condition; because the deviation is less than the threshold , there is also no transfer power through the interlinking converter.

Fig. 15 shows the experimental power waveforms about the output active power from ac and dc microgrids respectively. From the Fig, it can be found that at the first and second stage, the two microgrids can share the load in average and at the third and fourth stage, the two microgrids are not necessary to share the load in average. Fig. 16 shows the experimental power waveforms about the active power transferred by the interlinking converter. Fig. 17 and Fig. 18 show the per-unit values of the ac microgrid frequency and dc microgrid voltage, and the ac grid voltage, respectively. It could be easily found that proportional active power sharing was achieved and the p. u. values were also always the same and they can be restored to their nominal values.

It is worthwhile to remark here that the computation burden of the proposed DDMFAC scheme in our manuscript could be not really larger than other adaptive methods such as robust adaptive control, neural network adaptive control. In addition to the update equations, the uncertainty dynamics should be estimated for the robust adaptive control and large trainings are required in the neural adaptive control method. These also need considerable computational burden. Data driven MFAC method does not require a priori physical and mathematical knowledge of the system, training process, which allows small computational burden, easy implementation and application. In order to cut the computational burden, the parameters d_y and d_u could be selected properly according to practical scenarios.

VI. Conclusion

This paper investigates on coordinated power sharing issues of interlinked ac and dc microgrids. To realize proportional power sharing between ac and dc microgrids, a novel primary controller including a dual-droop controller and a data-driven model-free adaptive voltage controller has been firstly proposed in this paper. Following, a secondary control scheme has also been proposed to cooperate with each microgrid to restore the dc voltages and the ac frequency to their nominal values. Using the proposed scheme, the interlinking converter, just like the hierarchical controlled DG units, will have the

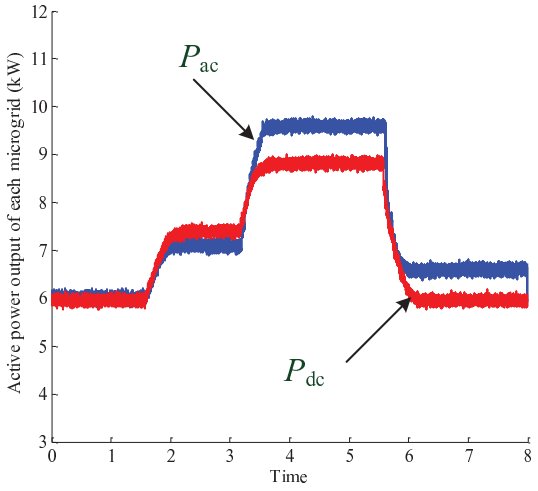

Fig. 15. The output active powers of the ac microgrid and the dc microgrid (W).

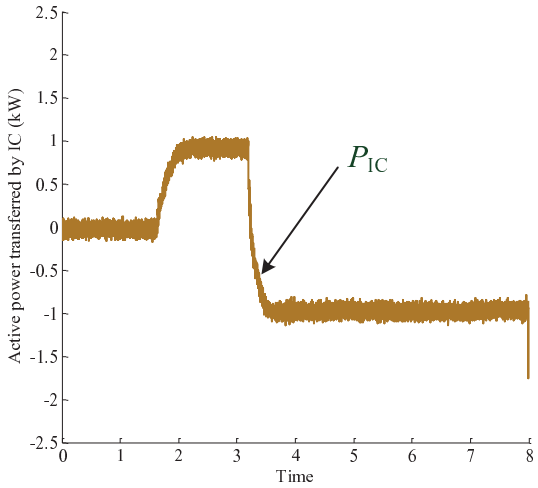

Fig. 16. The transferred active power by the interlinking converter (W).

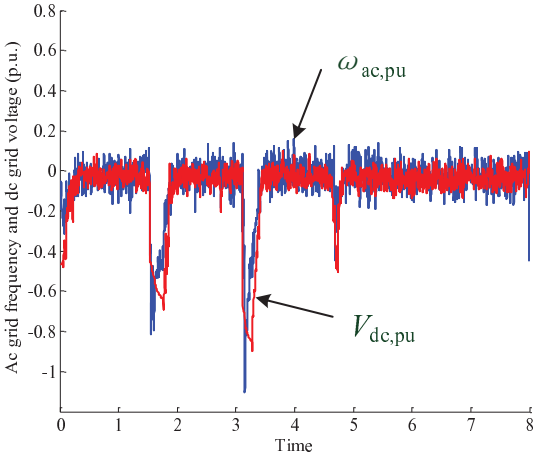

Fig. 17. The ac grid frequency and dc grid voltage (p.u.).

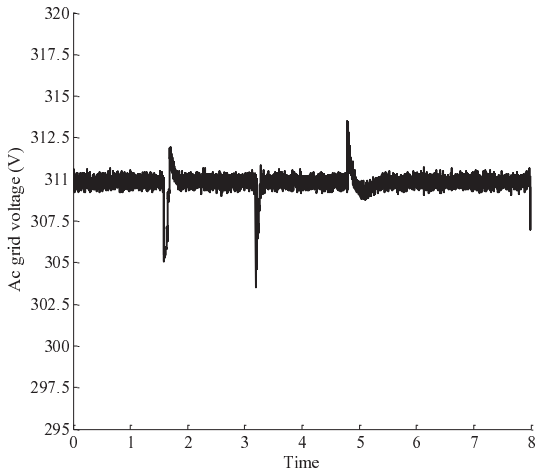

Fig. 18. The ac grid voltage (V).

ability to regulate and restore the dc terminal voltages and the ac frequency while keeping proportional power sharing. Moreover, the design of the controller is only based on input/output (I/O) measurement data but not the model any more. Simulation and experimental results have been given to verify the proposed power sharing strategy.

APPENDIX A

Variables in equation (4):

$\Delta \mathbf{U}(k) = \left[\Delta \mathbf{u}^T(k), \cdots, \Delta \mathbf{u}^T(k-L+1)\right]^T$,

$\Delta \mathbf{V}_i(k+1) = \mathbf{V}_i(k+1) - \mathbf{V}_i(k)$,

$\Delta \mathbf{u}(k-i+1) = \mathbf{u}(k-i+1) - \mathbf{u}(k-i), i = 1, \cdots, L$,

$$\mathbf{\Phi}_1(k) = \left[\begin{array}{ccc} \psi_1^{(L)^T}(k) & \psi_2^{(L)^T}(k) & \psi_3^{(L)^T}(k) \end{array}\right]^T = \left[\begin{array}{ccc} \phi_{11}^{(1)}(k) & \phi_{12}^{(1)}(k) & \phi_{13}^{(1)}(k) \quad \cdots \\ \phi_{21}^{(1)}(k) & \phi_{22}^{(1)}(k) & \phi_{23}^{(1)}(k) \quad \cdots \\ \phi_{31}^{(1)}(k) & \phi_{32}^{(1)}(k) & \phi_{33}^{(1)}(k) \quad \cdots \\ \phi_{11}^{(L)}(k) & \phi_{12}^{(L)}(k) & \phi_{13}^{(L)}(k) \\ \phi_{21}^{(L)}(k) & \phi_{22}^{(L)}(k) & \phi_{23}^{(L)}(k) \\ \phi_{31}^{(L)}(k) & \phi_{32}^{(L)}(k) & \phi_{33}^{(L)}(k) \end{array}\right],$$

$$\mathbf{\Phi}_2(k) = \left[\begin{array}{ccc} \phi_1^{(1)}(k) & \phi_2^{(1)}(k) & \phi_3^{(1)}(k) \quad \cdots \\ \phi_1^{(L)}(k) & \phi_2^{(L)}(k) & \phi_3^{(L)}(k) \end{array}\right], \text{ and}$$

$\|\mathbf{\Phi}_i(k)\| \leq C_i$, $C_i > 0$ are constants, L is a positive constant called control input length constant of linearization for the discrete-time nonlinear system.

Variables in equation (5): $\mathbf{K}_1 = diag(k_1, k_2, k_3)$, $\mathbf{K}_2 = K_2$, $\mathbf{\Gamma}_2(k) = \Gamma_4(k)$, $\mathbf{\Gamma}_1(k) = diag(\Gamma_1(k), \Gamma_2(k), \Gamma_3(k))$, $\Gamma_i(k) = 2\Big(\|\Delta \mathbf{U}(k)\|^2 + \mu_i\Big)^{-1}, i = 1, 2, 3, 4$, $\mathbf{F}_1 = diag(F_1, F_2, F_3)$, $\mathbf{F}_2 = F_4$, and $\tilde{\mathbf{V}}_i(k) = \mathbf{V}_i(k) - \hat{\mathbf{V}}_i(k)$.

APPENDIX B

Variables in equation (14):

$\Lambda_\sigma = \frac{k_{IC}\Delta\xi_{OL,t_k} - \frac{k_{dc}}{k_{ac}}\Delta\omega_{s,t_{k+1}} - \Delta V_{s,t_{k+1}}}{k_{IC}\Delta\xi_{OL,t_k} + \Delta V_{\omega,t_{k+1}}\tilde{\sigma}_{IC,t_k}}$, $k_{IC} = k_{ac} + k_{dc}$,

$\Lambda_k = \frac{k_{IC}\Delta\xi_{\min,t_k} - \frac{k_{dc}}{k_{ac}}\Delta\omega_{s,t_{k+1}} - \Delta V_{s,t_{k+1}}}{k_{IC}\Delta\xi_{\min,t_k} + \Delta V_{\omega,t_{k+1}}\tilde{k}_{IC,t_k}}$,

$\Delta\xi_{OL,t_k} = \xi_{s,t_k} - \xi_{OL}$, $\Delta\xi_{\min,t_k} = \xi_{s,t_k} - \xi_{\min}$, $\Delta\omega_{s,t_{k+1}} = \xi_{s,t_k} - \omega_{ac,pu,t_{k+1}}$, $\Delta V_{s,t_{k+1}} = \xi_{s,t_k} - V_{dc,pu,t_{k+1}}$, $\Delta V_{\omega,t_{k+1}} = V_{dc,pu,t_{k+1}} - \omega_{ac,pu,t_{k+1}}$.

APPENDIX C

TABLE I
SIMULATION TEST SYSTEM PARAMETERS

dc-microgrid	
Line-1	0.1 Ω
Line-2	0.1 Ω
Nominal voltage	650 V
ac-microgrid	
Line-3	0.05 Ω 0.25 mH
Line-4	0.05 Ω 0.25 mH
Nominal frequency	50 Hz
Nominal voltage	380 V (L-L)
Interlinking converter	
Filter inductance	3 mH
Filter capacitance	500 μF
dc-link capacitance	2200 μF
Parasitic resistance	0.01 Ω

TABLE II
SIMULATION PARAMETERS AND RANGES

dc-microgrid	
Maximum active power $P_{dc-\max}$	10 kW
Voltage range V_{dc}	640 V $< V_{dc} <$ 660 V
Droop coefficient k_{dc}	0.0002 W^{-1}
Secondary controller gains	$k_{pV} = 0.01$, $k_{iV} = 4\ s^{-1}$
ac-microgrid	
Maximum active power $P_{ac-\max}$	10 kW
Maximum reactive power $Q_{ac-\max}$	5 kVAr
Frequency range f_{ac}	49 Hz $\leq f_{ac} \leq$ 51 Hz
Droop coefficient k_{ac}	0.0002 W^{-1}
Secondary controller gains	$k_{p\omega} = 0.01$, $k_{i\omega} = 0.6\ s^{-1}$
Interlinking converter	
Frequency range	50.5 Hz $\leq f_{IC} \leq$ 51 Hz (0.5 p. u. $\leq f_{IC,pu} \leq$ 1 p. u.) (UL) 49.5 Hz $\leq f_{IC} \leq$ 50.5 Hz (-0.5 p. u. $\leq f_{IC,pu} \leq$ 0.5 p. u.) (NL) 49 Hz $\leq f_{IC} \leq$ 49.5 Hz (-1 p. u. $\leq f_{IC,pu} \leq$ -0.5 p. u.) (OL)
Voltage range	655 V $\leq V_{IC,dc} \leq$ 660 V (0.5 p. u. $\leq V_{IC,dc,pu} \leq$ 1 p. u.) (UL) 645 V $\leq V_{IC,dc} \leq$ 655 V (-0.5 p. u. $\leq V_{IC,dc,pu} \leq$ 0.5 p. u.) (NL) 640 V $\leq V_{IC,dc} \leq$ 645 V (-1 p. u. $\leq V_{IC,dc,pu} \leq$ -0.5 p. u.) (OL)
Controller parameters	$L = 3$ $diag(k_1, k_2, k_3) = diag(0.9, 0.9, 0.9)$ $K_2 = 0.9$ $diag(\alpha_1, \alpha_2, \alpha_3) = diag(0.3, 0.3, 0.3)$ $\alpha_4 = 0.15$

REFERENCES

[1] J. M. Guerrero, M. Chandorkar, T.-L. Lee, and P. C. Loh, "Advanced control architectures for intelligent microgrids-part I: decentralized and hierarchical control," *IEEE Trans. Ind. Electron.*, vol. 60, no. 4, pp. 1254-1262, Apr. 2013.

[2] C. Jin, P. Wang, J. Xiao, Y. Tang, and F. H. Choo, "Implementation of hierarchical control in dc microgrids," *IEEE Trans. Ind. Electron.*, vol. 61, no. 8, pp. 4032-4042, Aug. 2014.

TABLE III
EXPERIMENTAL SYSTEM PARAMETERS

ac/dc microgrids	
Power ratings of sources	$P_{ac-max} = 10$ kW (PV − arrays) $Q_{ac-max} = 3$ kVAr $P_{dc-max} = 10$ kW (PV : 5kW, WT : 5kW)
Voltage and frequency ranges	640 V< V_{dc} < 660 V 49 Hz < f_{ac} < 51 Hz
Droop coefficients	$k_{ac} = k_{dc} = 0.0002$ W^{-1}
Secondary controller gains	$k_{pV} = 0.015$, $k_{iV} = 3.9\ s^{-1}$ $k_{p\omega} = 0.011$, $k_{i\omega} = 0.62\ s^{-1}$
Feeder data	Line-1: R = 0.8 Ω Line-2: R = 0.5 Ω, L = 1.8 mH
Interlinking converter	
Filter inductance	1.8 mH
Filter capacitance	25 μF
dc-link capacitance	2200 μF
Controller parameters	$L = 2$ $diag\,(k_1, k_2, k_3) = diag\,(0.9, 0.9, 0.9)$ $K_2 = 0.9$ $diag\,(\alpha_1, \alpha_2, \alpha_3) = diag\,(0.3, 0.3, 0.3)$ $\alpha_4 = 0.15$

[3] N. Pogaku, M. Prodanovic, and T. C. Green, "Modeling, analysis and testing of autonomous operation of an inverter-based microgrid," *IEEE Trans. Power Electron.*, vol. 22, no. 2, pp. 613-625, Mar. 2007.

[4] Q. Sun, Y. Zhang, H. He, D. Ma, and H. Zhang, "A novel energy function based stability evaluation and nonlinear control for energy internet," *IEEE Trans. Smart Grid*, to be published.

[5] N. Bottrell, M. Prodanovic, and T. C. Green, "Dynamic stability of a microgrid with an active load," *IEEE Trans. Power Electron.*, vol. 28, no. 11, pp. 5107-5119, Nov. 2013.

[6] S. M. Ashabani and Y. A. R. I. Mohamed, "A flexible control strategy for grid-connected and islanded microgrids with enhanced stability using nonlinear microgrid stabilizer," *IEEE Trans. Smart Grid*, vol. 3, no. 3, pp. 1291-1301, Sep. 2012.

[7] T. L. Lee and P. T. Cheng, "Design of a new cooperative harmonic filtering strategy for distributed generation interface converters in an islanding network," *IEEE Trans. Power Electron.*, vol. 22, pp. 1919-1927, Sep. 2007.

[8] Q.-C. Zhong, and Y. Zeng, "Control of inverters via a virtual capacitor to achieve capacitive output impedance," *IEEE Trans. Power Electron.*, vol. 29, no. 10, pp. 5568-5578, Oct. 2014.

[9] J. He, Y. W. Li, and F. Blaabjerg, "Flexible microgrid power quality enhancement using adaptive hybrid voltage and current controller," *IEEE Trans. Ind. Electron.*, vol. 61, no. 6, pp. 2784-2794, Jun. 2014.

[10] Q.-C. Zhong, "Robust droop controller for accurate proportional load sharing among inverters operated in parallel," *IEEE Trans. Ind. Electron.*, vol. 60, no. 4, pp. 1281-1290, Apr. 2013.

[11] Q. Sun, J. Zhou, J. M. Guerrero, and H. Zhang, "Hybrid three-phase/single-phase microgrid architecture with power management capabilities," *IEEE Trans. Power Electron.*, vol. 30, no. 10, pp. 5964-5977, Oct. 2015.

[12] Q. Sun, R. Han, H. Zhang, J. Zhou, and J. M. Guerrero, "A multiagent-based consensus algorithm for distributed coordinated control of distributed generators in the energy internet," *IEEE Trans. Smart Grid*, vol. 6, no. 6, pp. 3006-3019, Nov. 2015.

[13] J. W. Simpson-Porco, F. Dorfler, and F. Bullo, "Synchronization and power sharing for droop-controlled inverters in islanded microgrids," *Automatica*, vol. 49, no. 9, pp. 2603-2611, Sep. 2013.

[14] U. Nutkani, P. C. Loh and F. Blaabjerg, "Distributed operation of interlinked AC microgrids with dynamic active and reactive power tuning," *IEEE Trans. Ind. Appl.*, vol. 49, no. 5, pp. 2188-2195, Sep. 2013.

[15] X. Liu, P. Wang, and P. C. Loh, "A hybrid ac/dc microgrid and its coordination control," *IEEE Trans. Smart Grid*, vol. 2, no. 2, pp. 278-286, Jun. 2011.

[16] P. C. Loh, D. Li, Y. K. Chai, and F. Blaabjerg, "Autonomous operation of hybrid microgrid with AC and DC subgrids," *IEEE Trans. Power Electron.*, vol. 28, no. 5, pp. 2214-2223, May 2013.

[17] P. C. Loh, D. Li, Y. K. Chai, and F. Blaabjerg, "Autonomous control of interlinking converter with energy storage in hybrid AC-DC microgrid," *IEEE Trans. Ind. Appl.*, vol. 49, no.3, pp. 1374-1382, May/Jun. 2013.

[18] P. C. Loh, D. Li, Y. K. Chai, and F. Blaabjerg, "Hybrid AC-DC microgrids with energy storages and progressive energy flow tuning," *IEEE Trans. Power Electron.*, vol. 28, no. 4, pp. 1533-1543, Apr. 2013.

[19] N. Eghtedarpour, and E. Farjah, "Power control and management in a hybrid AC/DC microgrid," *IEEE Trans. Smart Grid*, vol. 5, no. 3, pp. 1494-1505, May 2014.

[20] X. Lu, J.M. Guerrero, K. Sun, J. C. Vasquez, R. Teodorescu, and L. Huang, "Hierarchical control of parallel ac-dc converter interfaces for hybrid microgrids," *IEEE Trans. Smart Grid*, vol. 5, no. 2, pp. 683-692, Mar. 2014.

[21] H. Zhang, C. Qin, B. Jiang, and Y. Luo, "Online adaptive policy learning algorithm for H_∞ state feedback control of unknown affine nonlinear discrete-time systems," *IEEE Trans. Cybern.*, vol. 44, no. 12, pp. 2706-2718, Dec. 2014.

[22] H. Zhang, and Y. Quan, "Modeling, identification, and control of a class of nonlinear systems," *IEEE Trans. Fuzzy Syst.*, vol. 9, no. 2, pp. 349-354, Apr. 2001.

[23] A. H. Etemadi, E. J. Davison, and R. Iravani, "A decentralized robust control strategy for multi-DER microgrids-part I: fundamental concepts," *IEEE Trans. Power Del.*, vol. 27, no. 4, pp. 1843-1853, Oct. 2012.

[24] T. Geyer, and D. E. Quevedo, "Multistep finite control set model predictive control for power electronics," *IEEE Trans. Power Electron.*, vol. 29, no. 12, pp. 6836-6846, Dec. 2014.

[25] M. Davari, and Y. A.-R. I. Mohamed, "Variable-structure-based nonlinear control for the master VSC in dc-energy-pool multiterminal grids," *IEEE Trans. Power Electron.*, vol. 29, no. 11, pp. 6196-6213, Nov. 2014.

[26] H. Zhang, C. Qin, and Y. Luo, "Neural-network-based constrained optimal control scheme for discrete-time switched nonlinear system using dual heuristic programming," *IEEE Trans. Autom. Sci. Eng.*, vol. 11, no. 3, pp. 839-849, Jul. 2014.

[27] Z. Hou and S. Jin, "Data driven model-free adaptive control for a class of MIMO nonlinear discrete-time systems," *IEEE Trans. Neural Netw.*, vol. 22, no. 12, pp. 2173-2188, Dec. 2011.

[28] G. Rigatos, P. Siano, and N. Zervos, "Sensorless control of distributed power generators with the derivative-free nonlinear kalman filter," *IEEE Trans. Ind. Electron.*, vol. 61, no. 11, pp. 6369-6382, Nov. 2014.

[29] Q. Wei and D. Liu, "Data-driven neuro-optimal temperature control of water-gas shift reaction using stable iterative adaptive dynamic programming," *IEEE Trans. Ind. Electron.*, vol. 61, no. 11, pp. 6399-6408, Nov. 2014.

[30] H. Zhang, Y. Cui, X. Zhang, and Y. Luo, "Data-driven robust approximate optimal tracking control for unknown general nonlinear systems using adaptive dynamic programming method," *IEEE Trans. Neural Netw.*, vol. 22, no. 12, pp. 2226-2236, Dec. 2011.

[31] D. Xu, B. Jiang, and P. Shi, "A novel model-free adaptive control design for multivariable industrial processes," *IEEE Trans. Ind. Electron.*, vol. 61, no. 11, pp. 6391-6398, Nov. 2014.

[32] A. Q. Huang, M. L. Crow, G. T. Heydt, J. P. Zheng, and S. J. Dale, "The future renewable electric energy delivery and management system the Energy Internet," *IEEE Proceedings of the IEEE*, vol. 99, no. 1, pp. 133-148, Jan. 2011.

[33] Q. Shafiee, C. Stefanovic, T. Dragicevic, P. Popovski, J. C. Vasquez, and J. M. Guerrero, "Robust network control scheme for distributed secondary control of islanded microgrids," *IEEE Trans. Ind. Electron.*, vol. 61, no. 10, pp. 5363-5374, Oct. 2014.

[34] M. Ashabani, and Y. A.-R. I. Mohamed, "Novel comprehensive control framework for incorporating VSCs to smart power grids using bidirectional synchronous-VSC," *IEEE Trans. Power Syst.*, vol. 29, no. 2, pp. 943-957, Mar. 2014.

[35] A. A. A. Radwan, and Y. A.-R. I. Mohamed, "Assessment and mitigation of interaction dynamics in hybrid ac/dc distribution generation systems," *IEEE Trans. Smart Grid*, vol. 3, no. 3, pp. 1382-1393, Sep. 2012.

[36] F. Guo, C. Wen, J. Mao, and Y.-D. Song, "Distributed secondary voltage and frequency restoration control of droop-controlled inverter-based microgrids," *IEEE Trans. Ind. Electron.*, vol. 62, no. 7, pp. 4356-4364, Jul. 2015.

Huaguang Zhang (M'03-SM'04-F'14) received the B.S. degree and the M.S. degree in control engineering from Northeast Dianli University of China, Jilin City, China, in 1982 and 1985, respectively. He received the Ph.D. degree in thermal power engineering and automation from Southeast University, Nanjing, China, in 1991.

He joined the Department of Automatic Control, Northeastern University, Shenyang, China, in 1992, as a Postdoctoral Fellow for two years. Since 1994, he has been a Professor and Head of the Institute of Electric Automation, School of Information Science and Engineering, Northeastern University, Shenyang, China. His main research interests are fuzzy control, stochastic system control, neural networks based control, nonlinear control, and their applications. He has authored and coauthored over 280 journal and conference papers, six monographs and co-invented 90 patents.

Dr. Zhang is the fellow of IEEE, the E-letter Chair of IEEE CIS Society, the former Chair of the Adaptive Dynamic Programming & Reinforcement Learning Technical Committee on IEEE Computational Intelligence Society. He is an Associate Editor of AUTOMATICA , IEEE TRANSACTIONS ON NEURAL NETWORKS, IEEE TRANSACTIONS ON CYBERNETICS, and NEUROCOMPUTING, respectively. He was an Associate Editor of IEEE TRANSACTIONS ON FUZZY SYSTEMS (2008-2013). He was awarded the Outstanding Youth Science Foundation Award from the National Natural Science Foundation Committee of China in 2003. He was named the Cheung Kong Scholar by the Education Ministry of China in 2005. He is a recipient of the IEEE Transactions on Neural Networks 2012 Outstanding Paper Award.

Jianguo Zhou was born in Yunnan, China, in 1987. He received the B.S. degree in automation, and the M.S. degree in control theory and control engineering from the Northeastern University, Shenyang, China, in 2011 and 2013, respectively. He is currently working toward the Ph.D. degree in control theory and control engineering from the Northeastern University, Shenyang, China.

His current research interests includes power electronics, hierarchical and distributed cooperative control, and power quality improvement of microgrids, and synchronization of complex/multi-agent networks and their applications in microgrids and Energy Internet.

Qiuye Sun (M'-) received the B.S. degree in power system and its automaton from the Northeast Dianli University of China, Jilin City, China, in 2000, the M.S. degree in power electronics and drives, and the Ph.D. degree in control theory and control engineering from the Northeastern University, Shenyang, China, in 2004 and 2007, respectively. Since 2014, he has been a Full Professor with the School of Information Science and Engineering, Northeastern University, China.

His main research interests are Optimization Analysis Technology of Power Distribution Network, Network Control of Distributed Generation System, microgrids, and Energy Internet. He has authored and coauthored over 280 journal and conference papers, six monographs and co-invented 90 patents.

Josep M. Guerrero (S'01-M'04-SM'08-FM'15) received the B.S. degree in telecommunications engineering, the M.S. degree in electronics engineering, and the Ph.D. degree in power electronics from the Technical University of Catalonia, Barcelona, in 1997, 2000 and 2003, respectively. Since 2011, he has been a Full Professor with the Department of Energy Technology, Aalborg University, Denmark, where he is responsible for the Microgrid Research Program. From 2012 he is a guest Professor at the Chinese Academy of Science and the Nanjing University of Aeronautics and Astronautics; from 2014 he is chair Professor in Shandong University; and from 2015 he is a distinguished guest Professor in Hunan University.

His research interests is oriented to different microgrid aspects, including power electronics, distributed energy-storage systems, hierarchical and cooperative control, energy management systems, and optimization of microgrids and islanded minigrids. Prof. Guerrero is an Associate Editor for the IEEE TRANSACTIONS ON POWER ELECTRONICS, the IEEE TRANSACTIONS ON INDUSTRIAL ELECTRONICS, and the IEEE Industrial Electronics Magazine, and an Editor for the IEEE TRANSACTIONS on SMART GRID and IEEE TRANSACTIONS on ENERGY CONVERSION. He has been Guest Editor of the IEEE TRANSACTIONS ON POWER ELECTRONICS Special Issues: Power Electronics for Wind Energy Conversion and Power Electronics for Microgrids; the IEEE TRANSACTIONS ON INDUSTRIAL ELECTRONICS Special Sections: Uninterruptible Power Supplies systems, Renewable Energy Systems, Distributed Generation and Microgrids, and Industrial Applications and Implementation Issues of the Kalman Filter; and the IEEE TRANSACTIONS on SMART GRID Special Issue on Smart DC Distribution Systems. He was the chair of the Renewable Energy Systems Technical Committee of the IEEE Industrial Electronics Society. He received the 2014 best paper award of the IEEE Transactions on Energy Conversion. In 2014 and 2015 he was awarded by Thomson Reuters as Highly Cited Researcher, and in 2015 he was elevated as IEEE Fellow for his contributions on "distributed power systems and microgrids."

Dazhong Ma received the B.S. degree in automation, and the Ph.D. degree in control theory and control engineering from Northeastern University, Shenyang, China, in 2004 and 2011, respectively.

He is currently a Lecturer with Northeastern University. His current research interests include fault diagnosis, fault-tolerant controls, energy management systems, and control and optimization of distributed generation systems, microgrids and Energy Internet.